

Large Jet Multiplicities and New Physics at the LHC

Joseph Bramante*, Jason Kumar†, and Brooks Thomas‡

Department of Physics, University of Hawaii, Honolulu, HI 96822 USA

Abstract

A broad class of scenarios for new physics involving additional strongly-interacting fields generically predicts signatures at hadron colliders which consist solely of large numbers of jets and substantial missing transverse energy. In this work, we investigate the prospects for discovery in such scenarios using a search strategy in which jet multiplicity and missing transverse energy are employed as the primary criteria for distinguishing signal from background. We examine the discovery reach this strategy affords in an example theory (a simplified supersymmetric model whose low-energy spectrum consists of a gluino, a light stop, and a light neutralino) and demonstrate that it frequently exceeds the reach obtained via other, alternative strategies.

* E-mail address: bramante@hawaii.edu

† E-mail address: jkumar@hawaii.edu

‡ E-mail address: thomasbd@phys.hawaii.edu

I. INTRODUCTION

Determining how to identify and interpret signals of new physics within a rapidly accumulating store of LHC data has become one of the primary challenges for particle phenomenology of late. Particular attention has been focused on those signals which can be resolved within the first few fb^{-1} of integrated luminosity. These include signals due to new strongly-interacting particles, which can be produced copiously at hadron colliders via strong interactions. Since $SU(3)_c$ gauge invariance requires each of these particles to decay down to a final state including one or more Standard-Model (SM) quarks or gluons, theories which predict such new particles frequently lead to excesses in multi-jet events — excesses which can only be resolved above the sizeable SM QCD background via the application of astutely chosen event-selection criteria.

Nevertheless, while excesses in multi-jet events are a common prediction in models of new physics, the optimal search strategy¹ for resolving such new physics above a sizeable SM background depends on the features of the model. One strategy useful in a number of beyond-the-Standard-Model (BSM) contexts is to focus on channels in which additional particles, such as charged leptons, appear alongside the jets in the final state. Another is to search for multi-jet resonances arising from the decay of new strongly-interacting particles. Indeed, the utility of this strategy has been demonstrated in a variety of BSM contexts [1–3], and has recently been implemented, for example, in the trijet searches conducted by the CDF [4] and CMS [5] collaborations. Yet another fruitful strategy for resolving signals of new physics in multi-jet events is to search for events with substantial missing transverse energy (\cancel{E}_T). This strategy is particularly relevant in extensions of the SM which include not only additional strongly-interacting fields, but also a stable dark-matter candidate. In traditional dark-matter models, the stability of the dark matter candidate is frequently guaranteed by some symmetry, such as R-parity in supersymmetric theories, Kaluza-Klein parity [6] in models with universal extra dimensions [7–9] (UED), or T-parity [10] in little-Higgs theories [11]. Any other, heavier particle charged under the same symmetry, once produced, inevitably decays to a final state including one or more dark-matter particles, which manifest themselves at colliders as \cancel{E}_T . By contrast, only a minute fraction of events produced by pure QCD processes, which provide the dominant SM background for multi-jet events, include substantial \cancel{E}_T . This quantity therefore provides a useful discriminant between signal and background for multi-jet events in a variety of new physics models which include a stable dark-matter candidate (see, *e.g.*, Ref. [10, 12]). Searches for evidence of such models in the jets + \cancel{E}_T channel have been performed both at the Tevatron [13–15] and at the LHC [16–19]. Moreover, even in alternative dark-matter scenarios which do *not* include a single, stable dark-matter candidate [20], and indeed even in certain extensions of the SM which do not relate directly to the dark matter problem, the \cancel{E}_T can still play a crucial role in resolving signals of new physics.

In this paper, we examine the prospects for resolving a particular class of models which give rise to signals in the jets+ \cancel{E}_T channel: those in which the additional strongly-interacting fields decay preferentially to SM states involving third-generation quarks, and in particular

¹ The phrase “search strategy” has a range of meanings in common use. Here and throughout this paper, we use the phrase specifically to refer to the identification of particular channels relevant for the observation of new physics in the context of some extension of the Standard Model and the application of a particular set of event-selection criteria in order to resolve a signal of that new physics in those relevant channels.

top quarks. Such “top-rich” scenarios arise in a number of BSM contexts and give rise to a variety of distinctive signature patterns. Such signature patterns play a crucial role in the LHC phenomenology of these scenarios — especially in cases in which all relevant BSM fields decay essentially exclusively to states involving top quarks and invisible particles alone. A number of recent studies have assessed the prospects for detecting signals of new physics in top-rich scenarios which give rise to the specific event topologies $t\bar{t} + \cancel{E}_T$ [21, 22] and $t\bar{t}\bar{t} + \cancel{E}_T$ [23–25]. Most of these studies have focused on search strategies which require the presence of one or more charged leptons in the final state, in addition to jets and \cancel{E}_T . This approach has shown to be fruitful in many BSM contexts including supersymmetry (SUSY), in which the color-charged superpartners with complex decay chains generically produce final states of this sort.

In this paper, we examine an alternative strategy for resolving signals of new physics from the SM background in top-rich scenarios whose decay topologies are dominated by tops and invisible particles alone. This strategy involves focusing on the fully hadronic channel (*i.e.*, on events which include no high- p_T charged leptons), and selecting events primarily on the basis of two criteria: the number N_j of high- p_T jets in the event and the total missing transverse energy \cancel{E}_T .² There are many advantages to this approach. One of the principal ones is that the contribution to the SM background in the jets + \cancel{E}_T channel from pure QCD processes arises due to “fake” sources of \cancel{E}_T (*e.g.*, jet-energy mismeasurement), and several strategies (including those discussed in Refs. [27, 28], as well as a variety of data-driven techniques) exist for reducing this background to manageable levels. Moreover, the imposition of a charged-lepton veto can significantly suppress the sizeable SM backgrounds from $t\bar{t} + \text{jets}$ and $W + \text{jets}$ events involving one or more leptonically-decaying W bosons. These events often contain substantial \cancel{E}_T , due to the presence of one or more neutrinos in the final state, and consequently a substantial number of such events survive stringent \cancel{E}_T cuts imposed to eliminate the QCD background.

In order to demonstrate the utility of this search strategy for theories of this sort, we focus on a simplified model [32] whose field content includes a color-octet fermion, a color-triplet scalar, and a color-singlet fermion which plays the role of the dark-matter particle. This model can be realized within a certain limiting regime of the minimal supersymmetric Standard Model (MSSM). We find that within the context of this example model, a search strategy based principally on N_j and \cancel{E}_T turns out to be the optimal strategy for uncovering a signal of new physics at the LHC. Our results can also be readily adapted to a wide variety of qualitatively similar models via an appropriate rescaling of the pair-production cross-sections and decays widths of the particles involved. In many such cases, it is likely that a search based around these criteria will likewise be the optimal strategy for observing new physics.

Precedents for an analysis of this sort do exist in the literature in the context of particular models which give rise to top-rich event topologies, and it is encouraging to note that our claim is borne out in these cases. In Ref. [22], for example, the discovery potential for new physics was assessed in a model containing an exotic quark T' which decays directly to a top quark and a dark-matter particle with a branching fraction of effectively unity. It was shown that the best prospects for resolving a signal from the characteristic $t\bar{t} + \cancel{E}_T$ event topology which results from the pair-production of this T' were indeed obtained in the fully hadronic

² Top-rich scenarios also exist whose characteristic event topologies involve multiple top quarks, but no \cancel{E}_T . For such models, alternative search strategies [26] are required.

channel when minimum cuts on N_j and \cancel{E}_T were used as the primary event-selection criteria. This result has been confirmed by a recent CDF analysis [29]. The effectiveness of N_j and \cancel{E}_T cuts in resolving signals of new physics has also been demonstrated in the context of no-scale $\mathcal{F} - SU(5)$ models [30, 31], and the utility of such cuts in conjunction with additional event selection criteria was also demonstrated in Ref. [27]. We observe that many of the analysis techniques pioneered in these works are in fact applicable to a broad class of BSM theories which predict signatures with large jet multiplicities and substantial \cancel{E}_T .

The outline of this paper is as follows. In Sect. II, we review the production and decay properties of the gluino and lightest stop in our simplified model and discuss the top-rich event topologies to which the model gives rise. In Sect. III, we discuss the current limits on stop and gluino masses from Tevatron and LHC data, taking care to distinguish between those bounds which apply only when the masses of the first- and second-generation squarks are light and those which apply even in the limit in which those masses are taken to infinity. In Sect. IV, we enumerate the Standard Model backgrounds for a high-jet-multiplicity signal with substantial \cancel{E}_T and discuss the Monte-Carlo procedure adopted in our analysis. In Sect. V, we outline the program of event-selection criteria we employ in distinguishing such a signal from those backgrounds. In Sect. VI, we present our results for the LHC detection prospects for our simplified model and discuss how these results may be extended to other, related scenarios which likewise give rise to top-rich event topologies. Finally, in Sect. VII, we conclude.

II. LARGE JET MULTIPLICITIES FROM TOP-RICH EVENT TOPOLOGIES

The primary purpose of this paper is to examine the prospects for observing signals of new physics in high-jet-multiplicity events at hadron colliders afforded by adopting a search strategy focused on N_j and \cancel{E}_T . As noted above, this search strategy is of particular interest in top-rich scenarios and other theories whose decay phenomenologies are dominated by final states involving large numbers of high- p_T jets and invisible particles. In particular, our aim is to demonstrate the discovery reach which such a strategy is capable of achieving in scenarios of this sort within the first few fb^{-1} of integrated luminosity at the LHC, and to compare this reach to that afforded by alternative strategies. We work primarily within the context of a simplified model whose BSM field content includes only three new particles: a color-octet Majorana fermion, a color-triplet scalar, and a neutral, color-singlet fermion. These particles are assumed to transform under the symmetries of the theory identically to a gluino \tilde{g} , a single, effectively right-handed stop $\tilde{t}_1 \approx \tilde{t}_R$, and a light, bino-like neutralino $\tilde{N}_1 \approx \tilde{B}$ in the R -parity-conserving MSSM. For sake of convenience and to make contact with experimental limits extant in the literature, we shall henceforth refer to these particles by the corresponding sparticle names. However, our results apply to any theory with the same field content and charge assignments, whether or not that theory arises in the context of SUSY. Furthermore, we assume a mass hierarchy $M_{\tilde{g}}, m_{\tilde{t}_1} > m_{\tilde{N}_1}$ among these particles in what follows, and that \tilde{N}_1 is stable.

One of the primary advantages of adopting such a toy theory as an arena in which to study large-jet-multiplicity physics is that the decay behavior of both \tilde{g} and \tilde{t}_1 in this model is particularly simple. Under the assumption of minimal flavor violation, \tilde{t}_1 decays almost exclusively via $\tilde{t}_1 \rightarrow t\tilde{N}_1$ as long as this channel is kinematically open. Similarly, \tilde{g} decays almost exclusively through $\tilde{g} \rightarrow \tilde{t}_1 t \rightarrow t\bar{t}\tilde{N}_1$ and the conjugate process, where \tilde{t}_1 may be real

or virtual, depending on the relationship between $M_{\tilde{g}}$ and $m_{\tilde{t}_1}$. As a consequence of this simple decay phenomenology, each production process which contributes to the signal-event rate in the jets + \cancel{E}_T channel is characterized by a *distinctive* distribution of jet multiplicities. This example model therefore provides an excellent venue in which to assess the merits and drawbacks of a jet-multiplicity-based event-selection strategy for a variety of qualitatively different production and decay scenarios by scanning over the model-parameter space. Indeed, the qualitative results we obtain in the context of this model should be applicable in a wide variety of related scenarios characterized by similar decay phenomenologies and can therefore serve as a useful rubric for assessing whether a jet-multiplicity-based search strategy is the optimal strategy for obtaining a signal of new physics in any particular such model.

While our simplified model can be realized as a limiting case of the MSSM in which the masses of all other sparticles are infinitely heavy and decoupled, it is important to highlight the ways in which the collider phenomenology of this model differ from that realized in other regions of the parameter space of the general MSSM. With regard to the jets + \cancel{E}_T channel, a crucial distinction arises between the regime in which the remaining squarks (hereafter collectively denoted \tilde{q}) are heavy and decoupled and the regime in which one or more of these squarks have TeV-scale masses. Indeed, as we shall see in Sect. III, experimental limits on sparticle masses (and on $M_{\tilde{g}}$ in particular) differ significantly between these two regimes. It therefore behooves us to highlight the differences between MSSM scenarios with and without light squarks from the perspective of multi-jet collider phenomenology, before we move on to address \tilde{g} and \tilde{t}_1 production and decay in our toy theory.

The first significant distinction between SUSY scenarios with and without light \tilde{g} lies in the types of production processes which contribute non-trivially to the total event rate in the jets + \cancel{E}_T channel. In models in which the \tilde{q} are decoupled, there are only two such processes $pp \rightarrow \tilde{g}\tilde{g}$ and $pp \rightarrow \tilde{t}_1\tilde{t}_1^*$. Indeed, the only other contributions are those from $pp \rightarrow \tilde{g}\tilde{t}_1$ and its conjugate process. Under the assumption of minimal flavor violation, these contributions are suppressed by small off-diagonal elements in the Cabibbo-Kobayashi-Maskawa (CKM) matrix and may be safely neglected. By contrast, in models with light \tilde{q} , additional pair-production processes such as $pp \rightarrow \tilde{g}\tilde{q}$ and $pp \rightarrow \tilde{q}\tilde{q}^*$ also contribute. As a result, the N_j and \cancel{E}_T distributions which result from such models can differ significantly from those which result from models in which the \tilde{q} are heavy and decoupled.

A second difference between scenarios with and without light \tilde{q} arises due to the effect of these squarks on the cross-sections for those multi-jet-production processes which occur in both sorts of models. In decoupled models (again assuming minimal flavor violation), only the limited number of Feynman diagrams displayed in Fig. 1 contribute to $pp \rightarrow \tilde{g}\tilde{g}$ and $pp \rightarrow \tilde{t}_1\tilde{t}_1^*$. By contrast, in models in which one or more of the first- and second-generation squarks are light, additional diagrams involving the t -channel exchange of such squarks also contribute, and the inclusion of these additional diagrams can result in a significant modification of the production cross-section for $pp \rightarrow \tilde{g}\tilde{g}$ relative to that obtained in the decoupled-squark limit.

A third significant difference between the collider phenomenologies associated with decoupled and non-decoupled scenarios arises from differences in the decay properties of the gluino in these two scenarios. In the limit in which the \tilde{q} are decoupled, all decay chains initiated by \tilde{g} decay necessarily involve either a real or virtual \tilde{t}_1 , and hence lead to the production of a $t\bar{t}$ pair. Consequently, all fully hadronic final states resulting from $pp \rightarrow \tilde{g}\tilde{g}$ production necessarily include at least twelve “jets” (*i.e.*, quarks or gluons) at the parton

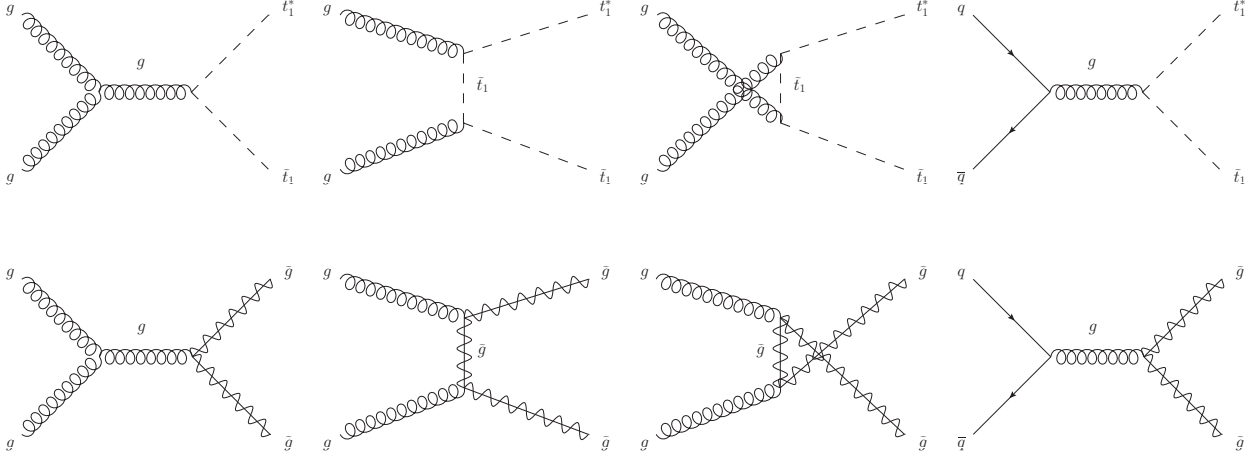


FIG. 1: Feynman diagrams associated with the processes relevant for \tilde{g} and \tilde{t}_1 pair-production in the limit in which all other squarks are taken to be heavy and decoupled.

level. This is generally not the case for models with light \tilde{q} . In particular, in scenarios in which $m_{\tilde{t}_1} > M_{\tilde{g}}$, and no two-body decay channels are open for the gluino, the branching fractions for three-body gluino-decay processes involving virtual \tilde{q} (such as $\tilde{g} \rightarrow q\tilde{q}\tilde{N}_1$, where q denotes any light quark) can be significant. As a consequence, the expected jet multiplicities from $pp \rightarrow \tilde{g}\tilde{g}$ in the fully hadronic channel can often be substantially lower in these scenarios than in those in which the \tilde{q} are decoupled. Moreover, we note that the decay phenomenology of both \tilde{g} and \tilde{t}_1 in the general MSSM are sensitive not only to the squark masses, but to the mass spectra of the chargino, neutralino, and slepton sectors as well.

Having highlighted some of the salient differences between our example model and other, similar models, we now examine its multi-jet phenomenology. As discussed above, the only contributions to the total event rate in the jets + \cancel{E}_T channel in our toy theory arise due to gluino-pair and stop-pair production. The cross-sections for the partonic gluino-production processes $gq \rightarrow \tilde{g}\tilde{g}$ and $q\bar{q} \rightarrow \tilde{g}\tilde{g}$ are given at leading order (LO) by [33, 34]

$$\begin{aligned}\hat{\sigma}_{q\bar{q} \rightarrow \tilde{g}\tilde{g}}(\hat{s}) &= \frac{8\pi\alpha_s^2}{9\hat{s}} \left(1 + \frac{2M_{\tilde{g}}^2}{\hat{s}}\right) R \\ \hat{\sigma}_{gg \rightarrow \tilde{g}\tilde{g}}(\hat{s}) &= \frac{3\pi\alpha_s^2}{4\hat{s}} \left[3 \left(1 + \frac{4M_{\tilde{g}}^2}{\hat{s}} - \frac{4M_{\tilde{g}}^4}{\hat{s}^2}\right) \ln\left(\frac{1+R}{1-R}\right) - \left(4 + \frac{17M_{\tilde{g}}^2}{\hat{s}}\right) R\right],\end{aligned}\quad (1)$$

where $R \equiv \sqrt{1 - 4M_{\tilde{g}}^2/\hat{s}}$. Similarly, the partonic cross-sections for the corresponding stop-pair production processes are given by [33]

$$\begin{aligned}\hat{\sigma}_{q\bar{q} \rightarrow \tilde{t}_1\tilde{t}_1^*}(\hat{s}) &= \frac{2\pi\alpha_s^2}{27\hat{s}} S^3 \\ \hat{\sigma}_{gg \rightarrow \tilde{t}_1\tilde{t}_1^*}(\hat{s}) &= \frac{\pi\alpha_s^2}{6\hat{s}^2} \left[\left(\frac{5}{8} + \frac{31m_{\tilde{t}_1}^2}{4\hat{s}}\right) \hat{s}S - \left(4 + \frac{m_{\tilde{t}_1}^2}{\hat{s}}\right) m_{\tilde{t}_1}^2 \ln\left(\frac{1+S}{1-S}\right) \right],\end{aligned}\quad (2)$$

where $S \equiv \sqrt{1 - 4m_{\tilde{t}_1}^2/\hat{s}}$.

In Fig. 2, we indicate how the total (LO) cross-sections $\sigma_{pp \rightarrow \tilde{g}\tilde{g}}$ and $\sigma_{pp \rightarrow \tilde{t}_1 \tilde{t}_1^*}$ for gluino- and stop-pair production at the $\sqrt{s} = 7$ TeV LHC behave as functions of $M_{\tilde{g}}$ and $m_{\tilde{t}_1}$. The curves appearing in this figure were obtained by convolving the partonic cross-section formulae in Eqs. (1) and (2) with the CTEQ6L1 [35] parton-distribution function (PDF) set and approximating the running of α_s using the relation

$$\alpha_s(Q) = \alpha_s(M_Z) \left(1 + \frac{\alpha_s(M_Z)}{12\pi} \left[23 - 2\Theta(Q^2 - m_t^2) \ln \left(\frac{Q^2}{m_t^2} \right) - 6\Theta(Q^2 - M_{\tilde{g}}^2) \ln \left(\frac{Q^2}{M_{\tilde{g}}^2} \right) - \frac{1}{2}\Theta(Q^2 - m_{\tilde{t}_1}^2) \ln \left(\frac{Q^2}{m_{\tilde{t}_1}^2} \right) - \frac{11}{2}\Theta(Q^2 - m_{\tilde{q}}^2) \ln \left(\frac{Q^2}{m_{\tilde{q}}^2} \right) \right] \right)^{-1}, \quad (3)$$

where $\Theta(x)$ is the Heaviside theta function, Q is the energy scale at which the coupling is being evaluated, and m_t is the top-quark mass (taken here to be $m_t = 172$ GeV). The fiducial value $\alpha_s(M_Z) = 0.130$ assigned to α_s at the weak scale was chosen to accord with the definition in the CTEQ6L1 PDF set.

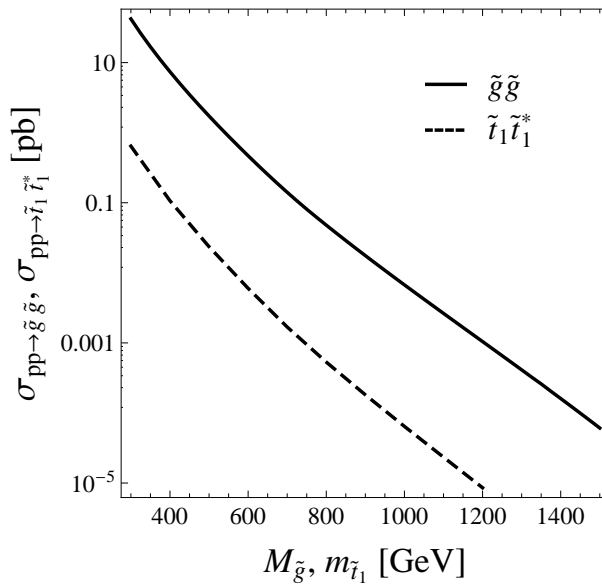


FIG. 2: Total LO cross sections $\sigma_{pp \rightarrow \tilde{g}\tilde{g}}$ (solid curve) and $\sigma_{pp \rightarrow \tilde{t}_1 \tilde{t}_1^*}$ (dashed curve) at the $\sqrt{s} = 7$ TeV LHC in the limit in which all other squark masses are taken to infinity.

Since next-to-leading order (NLO) corrections to the cross-sections for both $pp \rightarrow \tilde{g}\tilde{g}$ and $pp \rightarrow \tilde{t}_1 \tilde{t}_1^*$ production can be quite significant, we also account for the effects of such corrections. We approximate these effects by scaling our leading-order results for $\sigma_{pp \rightarrow \tilde{g}\tilde{g}}$ and $\sigma_{pp \rightarrow \tilde{t}_1 \tilde{t}_1^*}$ by the overall multiplicative factors $K_{\tilde{g}\tilde{g}}^{\text{NLO}}$ and $K_{\tilde{t}_1 \tilde{t}_1^*}^{\text{NLO}}$ shown in Fig. 3, which incorporate the effects of NLO modifications. These NLO K -factors were evaluated for each combination of $M_{\tilde{g}}$ and $m_{\tilde{q}}$ included in our analysis using the Prospino package [36]. While the K -factor formalism employed here does not account for changes in kinematical distributions of the decay products of the gluino, some information on how these distributions

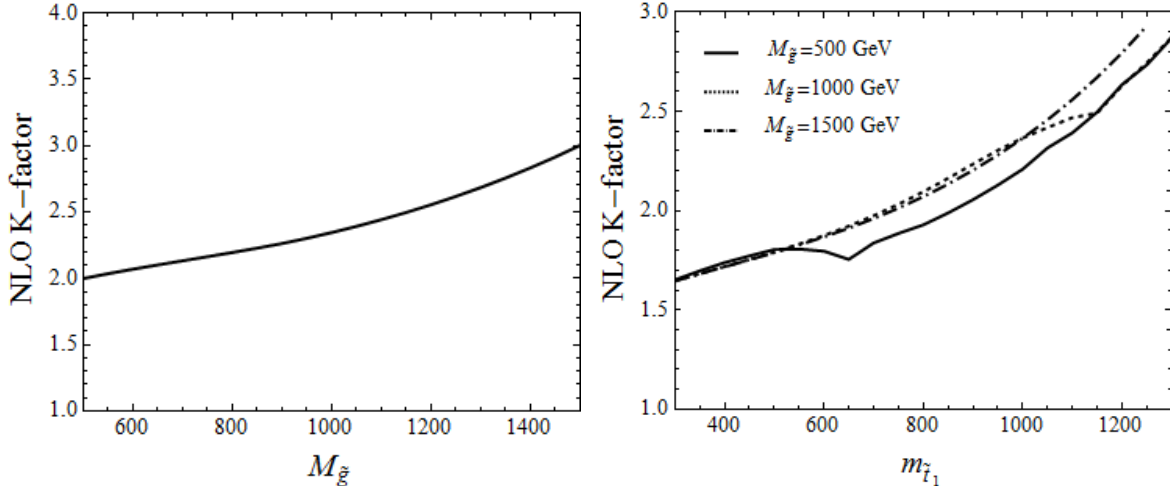


FIG. 3: The NLO K -factors for gluino-pair production (left panel) and stop-pair production (right panel) at a $\sqrt{s} = 7$ TeV LHC, shown as a function of the gluino mass $M_{\tilde{g}}$ and stop mass $m_{\tilde{t}_1}$, respectively. The results shown assume that all other squarks \tilde{q} are infinitely heavy and decoupled. The different curves in the right panel correspond to different choices of $M_{\tilde{g}}$.

are affected at NLO can be found in Ref. [38]. In this analysis, we do not include the effect of next-to-leading-log (NLL) corrections to these process from soft-gluon radiation, but we note that these corrections can provide an additional contribution as high as $\mathcal{O}(20\%)$ [37] to the total production cross-section in some cases.

III. CURRENT CONSTRAINTS

In this section, we summarize the collider constraints on $M_{\tilde{g}}$ and $m_{\tilde{t}_1}$ in our example model. We note that this summary not only delimits the viable parameter space of that model, but also provides a rough sense of the discovery reach for top-rich scenarios afforded by the search strategies employed in the corresponding analyses.

A number of new-physics searches place limits on $M_{\tilde{g}}$ and $m_{\tilde{t}_1}$ in our example scenario. One example is the recent search performed by the ATLAS collaboration [40] at an integrated luminosity $\mathcal{L}_{\text{int}} = 35 \text{ pb}^{-1}$. This analysis, focused on events containing one lepton and two high- p_T jets (one of which was required to be b -tagged). For $m_{\tilde{t}_1}$ in the range $130 \text{ GeV} \lesssim m_{\tilde{t}_{1,2}} \lesssim 300 \text{ GeV}$, the collaboration obtained a limit $M_{\tilde{g}} \geq 520 \text{ GeV}$ on the gluino mass. Likewise, limits on $m_{\tilde{t}_1}$ can be derived from the results of recent CDF searches for an exotic color-triplet fermion ψ which decays preferentially to a top quark and a scalar dark-matter candidate χ . Search results in the semileptonic channel [41] imply a bound $m_\psi \geq 360 \text{ GeV}$ on the mass of such a fermion, assuming $m_\chi \leq 100 \text{ GeV}$, while corresponding search results in the fully hadronic channel [29] imply a slightly more stringent lower limit $m_\psi \gtrsim 380 - 400 \text{ GeV}$ for m_χ within this mass range (the precise lower bound depending on m_χ). By taking into account the difference between the pair-production cross-sections for scalars and fermions, one can translate this bound into a rough lower limit $m_{\tilde{t}_1} \gtrsim 285 \text{ GeV}$ in our example model, under the same assumption about m_χ . A similar search performed by the Atlas collaboration [42] in the semileptonic channel at $\mathcal{L}_{\text{int}} = 35 \text{ pb}^{-1}$ yields the constraints $m_\psi \geq 275 \text{ GeV}$ and $m_\psi \geq 300 \text{ GeV}$ for $m_\chi = 50 \text{ GeV}$ and $m_\chi = 10 \text{ GeV}$,

respectively. Again accounting for the difference in production cross-section between scalars and fermions, we obtain the corresponding limits $m_{\tilde{t}_1} \gtrsim 190$ GeV and $m_{\tilde{t}_1} \gtrsim 215$ GeV in our example model for the corresponding choices of m_χ . A recent update [43] with $\mathcal{L}_{\text{int}} = 1.04 \text{ fb}^{-1}$ has elevated this lower limit to $m_{\tilde{t}_1} \gtrsim 270$ GeV for $m_\chi = 10$ GeV. The CDF [44] and DØ [45] collaborations have also performed searches for evidence of stop-pair production in the fully leptonic channel at $\mathcal{L}_{\text{int}} = 1 \text{ fb}^{-1}$. The non-observation of a signal at either experiment implies a bound $m_{\tilde{t}_1} \geq 180$ GeV (assuming that the dark matter particle is lighter than 100 GeV). CDF has conducted another search [46] at $\mathcal{L}_{\text{int}} = 2.7 \text{ fb}^{-1}$ for $\tilde{t}\tilde{t}^*$ production followed by the decay $\tilde{t} \rightarrow b\chi_1^\pm \rightarrow b\nu\chi_1^0$. The results of this search imply a limit $m_{\tilde{t}_1} \geq 150 - 185$ GeV in the context of our example model.

In addition to these constraints on top-rich scenarios, a number of other well-publicized limits on stop and gluino masses in SUSY theories (and in the MSSM in particular) had been derived from Tevatron and LHC data. For example, the ATLAS collaboration has searched for evidence of squark and gluino production in final states involving one isolated charged lepton, at least three high- p_T jets (with no b -tagging requirement), and \cancel{E}_T [39]. The results of this search, interpreted in the context of the constrained minimal supersymmetric Standard Model (CMSSM) with $A_0 = 0$, $\mu > 0$ and $\tan\beta = 3$, yield the constraint $M_{\tilde{g}} \geq 700$ GeV. A number of searches conducted at both the Tevatron and the LHC in the jets+ \cancel{E}_T channel serve to constrain $M_{\tilde{g}}$ as well. A recent CDF study [14] of this sort, performed at $\mathcal{L}_{\text{int}} = 2 \text{ fb}^{-1}$, used the results of such a search to derive a limit $M_{\tilde{g}} > 280$ GeV in the context of minimal supergravity (mSUGRA) in the $m_{\tilde{q}} \gg M_{\tilde{g}}$ limit (in which gluino-pair production dominates the signal rate) for the mSUGRA parameter assignments $\mu < 0$, $A_0 = 0$, and $\tan\beta = 5$. Corresponding DØ search results [13], performed at a similar \mathcal{L}_{int} and with similar mSUGRA parameter choices, imply a similar bound $M_{\tilde{g}} > 308$ GeV. An analogous study has also been performed by the CMS collaboration [16] at $\mathcal{L}_{\text{int}} = 35 \text{ pb}^{-1}$. Searches which do not assume a CMSSM or mSUGRA sparticle spectrum have also been performed at the LHC in the jets + \cancel{E}_T channel. A recent ATLAS study of this sort [18], performed at $\mathcal{L}_{\text{int}} = 165 \text{ pb}^{-1}$, focused on the case in which the third-generation squarks were taken to be extremely heavy, while the first- and second-generation squarks were taken to have TeV-scale masses. For simplicity, the lightest neutralino was treated as massless. For the case in which the first- and second-generation squarks are reasonably heavy, with masses around 2 TeV, a bound $M_{\tilde{g}} \geq 725$ GeV was obtained.

One might assume that the results of these searches, which generally impose far more stringent limits than the constraints on top-rich models quoted above, further serve to constrain the parameter space of our example model or place similar limits on other theories which also give rise almost exclusively to top-rich event topologies. However, these general SUSY results turn out not to be directly applicable to our example model. This is because the sparticle-mass spectra and decay phenomenologies of other SUSY scenarios often differ considerably from those obtained in that model, as discussed in Sect. II. For example, decay channels for squarks and gluinos which yield additional final-state leptons (beyond those produced from top decay) are often open in such scenarios. Moreover, the \tilde{q} generally play a significant role in the collider phenomenology of general MSSM and CMSSM scenarios, whereas in our example model such squarks play no role whatsoever. The stringent constraints on such scenarios we have quoted above are predicated on the effects of TeV-scale sparticles other than \tilde{g} , \tilde{t}_1 , and \tilde{N}_1 . In the absence of such effects, such constraints do not apply. Likewise, the discovery reach associated with typical search strategies for squarks and gluinos is considerably lower. However, as we demonstrate below, a hadronic-channel

analysis focused on N_j and \cancel{E}_T can yield a significant increase in the discovery reach for top-rich scenarios whose collider phenomenology is dominated by final states involving top quarks and \cancel{E}_T alone.

IV. STANDARD MODEL BACKGROUNDS AND EVENT GENERATION

We now discuss the SM processes which contribute to the background for large-jet-multiplicity searches in the jets + \cancel{E}_T channel at the LHC. The dominant contributions come from processes such as $t\bar{t}$ + jets and W^\pm + jets, with all heavy particles decaying hadronically, and from processes such as Z + jets and $t\bar{t}Z$ + jets in which the Z boson decays to a neutrino pair. In addition, a sizeable contribution arises from pure QCD processes in which the appearance of substantial \cancel{E}_T arises due to jet-energy mismeasurement, and from $W \rightarrow \tau\nu_\tau$ decays where the τ is mistagged as a jet.

In order to quantitatively assess the potential for resolving a signal of new physics above these backgrounds in the context of our toy theory, we perform a Monte-Carlo analysis. In simulating the signal data, we fix $M_{\tilde{N}_1} = 100$ GeV and survey over a range of stop and gluino masses from $300 \text{ GeV} \leq m_{\tilde{t}_1} \leq 1200 \text{ GeV}$ and $500 \text{ GeV} \leq M_{\tilde{g}} \leq 1500 \text{ GeV}$ in increments of 50 GeV. For each parameter-space point surveyed, a complete model was obtained using the SuSpect 2.41 package [47], and an NLO K -factor for each signal process was obtained using Prospino [36], as discussed in Sect. II. Events for both signal processes were then generated using the MadGraph/MadEvent package [48] (with the CTEQ6L1 [35] PDF set) for each point included in the survey and subsequently passed to Pythia 6.4.22 [49] for fragmentation and hadronization. Realistic detector effects were simulated using PGS4 [50], with detector parameters specified by the ATLAS detector card.

In this study, we do not simulate the QCD multi-jet background. Instead, we refer to the analyses performed in Refs. [51, 52], which demonstrate that this background can be reduced to negligible levels via the application of appropriate cuts on N_j , \cancel{E}_T , and the separation $\Delta\phi(p_{T_j}, \cancel{p}_T)$ in azimuthal angle between the most energetic jets and the missing-transverse-momentum vector \cancel{p}_T . In light of these results, we incorporate a similar set of cuts into our preliminary event-selection criteria (*i.e.*, the “precuts” detailed below) and assume that these cuts will likewise render the QCD background negligible. The remaining backgrounds from $t\bar{t}$ + jets, W^\pm + jets, Z + jets, and $t\bar{t}Z$ + jets were explicitly simulated using the Monte-Carlo procedure outlined above for signal-event generation, with matrix-element/parton-shower matching applied for each process in the inclusive samples. The W^\pm + jets and Z + jets background events were generated assuming at least three jets present at the parton level. While additional processes such as $t\bar{t}t\bar{t}$ + jets also contribute to the total SM multi-jet background, the cross-sections for these processes at the $\sqrt{s} = 7$ TeV LHC are small enough that they may be neglected.

Since NLO corrections to both $pp \rightarrow \tilde{g}\tilde{g}$ and $pp \rightarrow \tilde{t}_1\tilde{t}_1^*$ can be significant, such corrections must be applied to our background cross-sections as well. As with the signal, we account for NLO corrections to the SM backgrounds using the K -factor formalism. Specifically, we scale the production cross-section for each background process by the NLO K -factor associated with the partonic process with the lowest jet multiplicity included in the Monte-Carlo simulation of that background. This procedure is expected to yield a conservative estimate of the overall signal significance, since $t\bar{t}$ + jets provides the dominant contribution to the SM background after a substantial cut on N_j is applied, and since the K -factors for the subprocesses which contribute toward the inclusive cross-section for $t\bar{t}$ + jets tends to

Process	σ_{LO} (precuts)	$K_{\text{NLO}}(\mu)$	μ	\sqrt{s}
$t\bar{t}$ + jets	267.2 fb	1.40	m_t	14 TeV
W^\pm + jets	60.4 fb	0.65	M_W	7 TeV
Z + jets	48.6 fb	1.17	M_Z	7 TeV
$t\bar{t}Z$ + jets	0.7 fb	1.35	$m_t + M_Z/2$	14 TeV

TABLE I: Leading-order cross-sections σ_{LO} for each of the relevant SM background processes considered in this analysis after the application of the precuts discussed in Sect. V, as well as the NLO K -factor $K_{\text{NLO}}(\mu)$ associated with each process. The factorization and renormalization scales at which each K -factor has been evaluated are taken to be $\mu_F = \mu_R = \mu$, where the value of μ for each process, along with the center-of-mass energy \sqrt{s} for which each K -factor appearing in this table has been derived, are also displayed.

decrease as the number of jets involved increases. The NLO K -factors for several Z +jets [53] and W +jets [54] subprocesses have recently been computed for the LHC at a center-of-mass energy $\sqrt{s} = 7$ TeV. While corresponding results for the remaining processes included in our analysis are not yet extant in the literature for the same center-of-mass energy, K -factors for a number of $t\bar{t}$ +jets subprocesses [55, 56], as well as for $t\bar{t}Z$ +jets [57], have been computed at $\sqrt{s} = 14$ TeV. We estimate the K -factors for these processes by adopting these results. Numerical values for all K -factors used in this analysis are summarized in Table I, along with the center-of-mass energy and common factorization and renormalization scale μ at which each is evaluated. The LO cross-sections for the corresponding background processes (after the application of the precuts described in Sect. V below) are also included in the table.

Estimates of the SM backgrounds obtained from Monte-Carlo simulations should always be taken with a grain of salt, especially when those estimates apply to regimes (such as the large-jet-multiplicity regime) for which little experimental data exist to corroborate them. More accurate characterizations of the backgrounds relevant in these regimes will come as more experimental data are accumulated. However, preliminary studies based on simulations of this sort are frequently invaluable, as it is often in such regimes that signals of new physics can be most readily resolved. Moreover, the primary results of our analysis (for example, the projected discovery reach for $M_{\tilde{g}}$ and $m_{\tilde{t}_1}$) are not particularly sensitive to these uncertainties.

V. SURVEYING THE PARAMETER SPACE

Having examined the individual signal and background processes which contribute to the total event rate in the jets + \cancel{E}_T channel in our example scenario, we now outline the strategy we adopt for differentiating signal from background events in this channel — a strategy in which the principal event-selection criteria are N_j and \cancel{E}_T . In this analysis, N_j is specifically defined to be the number of jets in the event with $p_T > 30$ GeV. As we shall see, this strategy actually renders the fully-hadronic channel even more auspicious for discovery in our example model than other, more conventional channels. However, since our primary aim in this paper is to assess the efficacy of a search strategy based primarily on N_j and \cancel{E}_T for top-rich scenarios in general, rather than this example model in particular, we do not

optimize our event-selection criteria for each combination of the model parameters $M_{\tilde{g}}$, $m_{\tilde{t}_1}$, and $M_{\tilde{N}_1}$; but rather introduce a small number of representative cutting regimens, each of which is particularly effective within a certain characteristic region of model parameter space. We emphasize that none of the cuts we impose as part of this program of event-selection criteria involve b -tagging or top reconstruction. Indeed, since the dominant contribution to the SM background at large jet multiplicities is $t\bar{t}$ +jets, any further selection of events based on these techniques would reduce signal and background proportionally, and thus only serve to diminish signal significance.

As a first step in our event-selection procedure, we apply a preliminary set of cuts, hereafter referred to as our “precuts,” to both the signal and background data. These precuts are designed to mimic a realistic detector acceptance and to eliminate the sizable SM backgrounds from pure QCD processes, as discussed in Sect. IV, and from low-jet-multiplicity events in general. In particular, we require that all events satisfy the following criteria:

- No isolated charged leptons (e or μ) in the final state.
- At least five jets with $p_{T_j} > 40$ GeV.
- Each jet must be isolated in the sense that $\Delta R_{jj} > 0.4$ for every possible pairing of jets in the event, where ΔR_{jj} is the separation distance in the (η, ϕ) plane between a given pair of jets.
- An azimuthal-angle separation $\Delta\phi(p_{T_j}, \cancel{p}_T) > 11.5^\circ$ between the missing-transverse-momentum vector and each of the leading three jets (ranked by p_{T_j}).
- $\cancel{E}_T > 100$ GeV.

For the SM backgrounds, the only significant sources of missing energy are neutrinos and jet-energy mismeasurement. The first of these is suppressed quite efficiently by the lepton veto, while the second is suppressed by the combination of the minimum \cancel{E}_T cut and the requirement that the missing-transverse momentum vector \cancel{p}_T not be aligned (or anti-aligned) with any of the leading jets in a given event — the jets for which the potential for jet-energy mismeasurement is the greatest. It is worth noting that the $\Delta\phi(p_{T_j}, \cancel{p}_T)$ cut employed here differs from the $\Delta\phi^*$ and α_T cuts employed in Refs. [19, 58] for a similar purpose. As was pointed out in Refs. [30, 31], these latter variables may not be optimal for searches involving very large numbers of jets. By contrast our $\Delta\phi(p_{T_j}, \cancel{p}_T)$ cut, excludes events based on the proximity of the \cancel{p}_T vector to the three highest- p_T jets (for which the potential for jet-energy mismeasurement is the greatest) rather than the nearest jet, and may therefore be a more reliable variable in the large-jet-multiplicity regime.

We now consider the effect of imposing elevated cuts on N_j and \cancel{E}_T beyond those imposed in our precuts. In order to illustrate the effect that such additional cuts have on the statistical significance for discovery in this example model, we display the event distributions for all relevant signal and background processes as functions of N_j and \cancel{E}_T in Figs. 4 and 5 respectively. In both of these figures, each distribution shown has been normalized so that the total area under the distribution is unity.

The results displayed in Fig. 4 correspond to $M_{\tilde{g}} = 1000$ GeV and $m_{\tilde{t}_1} = 600$ GeV; however, the shapes of the N_j distributions for the signal processes do not vary significantly over the range of parameter space surveyed, primarily because N_j depends primarily on the

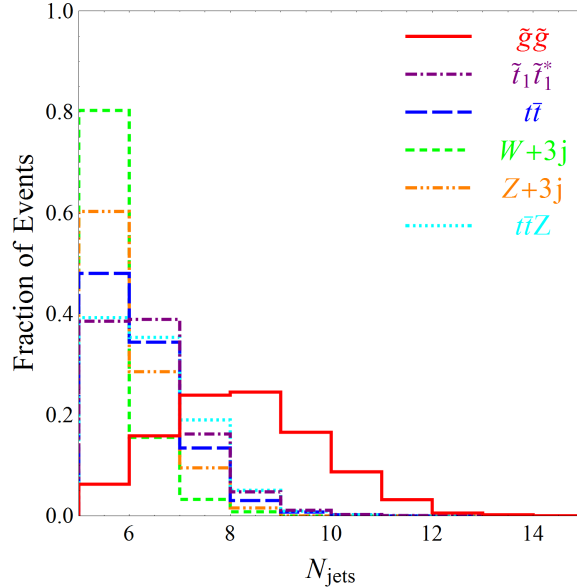


FIG. 4: Event distributions for all relevant signal and background processes as functions of jet number N_j corresponding to the parameter choice $M_{\tilde{g}} = 1000$ GeV and $m_{\tilde{t}_1} = 600$ GeV in our simplified supersymmetric model. Each distribution shown has been normalized so that the total area under it is unity.

structure of the decay chain and is not particularly sensitive to the details of the kinematics involved. For example, as discussed in Sect. II, the characteristic number of “jets” at the parton level (*i.e.*, final-state quarks or gluons) expected in the fully-hadronic channel from the $pp \rightarrow \tilde{g}\tilde{g}$ and $pp \rightarrow \tilde{t}_1\tilde{t}_1^*$ signal processes is twelve and six, respectively. The characteristic jet multiplicity for $pp \rightarrow \tilde{g}\tilde{g}$ at the detector level is reduced somewhat because the sheer number of quarks and gluons in the final state makes it increasingly likely that multiple such partons will be clustered together into the same jet. Nevertheless, this process clearly yields a substantial number of events with large N_j . We also remark that while the results shown in Fig. 4 correspond to a situation in which $M_{\tilde{g}} > m_t + m_{\tilde{t}_1}$, the N_j distributions for $pp \rightarrow \tilde{g}\tilde{g}$ do not differ drastically from these even in cases in which $M_{\tilde{g}} < m_t + m_{\tilde{t}_1}$ and gluino decay proceeds via an off-shell stop. By contrast, the largest contributions to the SM background from $t\bar{t} + \text{jets}$ and $W^\pm + \text{jets}$ after the application of the precuts are those from events in which a W^\pm boson decays to a τ lepton, which is misidentified as a jet, and a neutrino. These backgrounds exhibit far lower characteristic jet multiplicities. Indeed, only a minute fraction of background events surviving our precuts have $N_j \geq 8$, whereas roughly half of the $pp \rightarrow \tilde{g}\tilde{g}$ events contain at least this number of jets. This figure therefore attests to how effective an elevated N_j cut can be in discriminating between signal and background in regions of parameter space in which gluino-pair production provides the largest contribution to the signal.

The results shown in Fig. 5 likewise motivate the application of an elevated \cancel{E}_T cut in certain cases, although the utility of such a cut is more sensitive to the values of $M_{\tilde{g}}$ and $m_{\tilde{t}_1}$. The distributions displayed in the left panel of the figure correspond to the parameter assignments $M_{\tilde{g}} = 800$ GeV and $m_{\tilde{t}_1} = 600$ GeV. For this choice of parameters, as can be

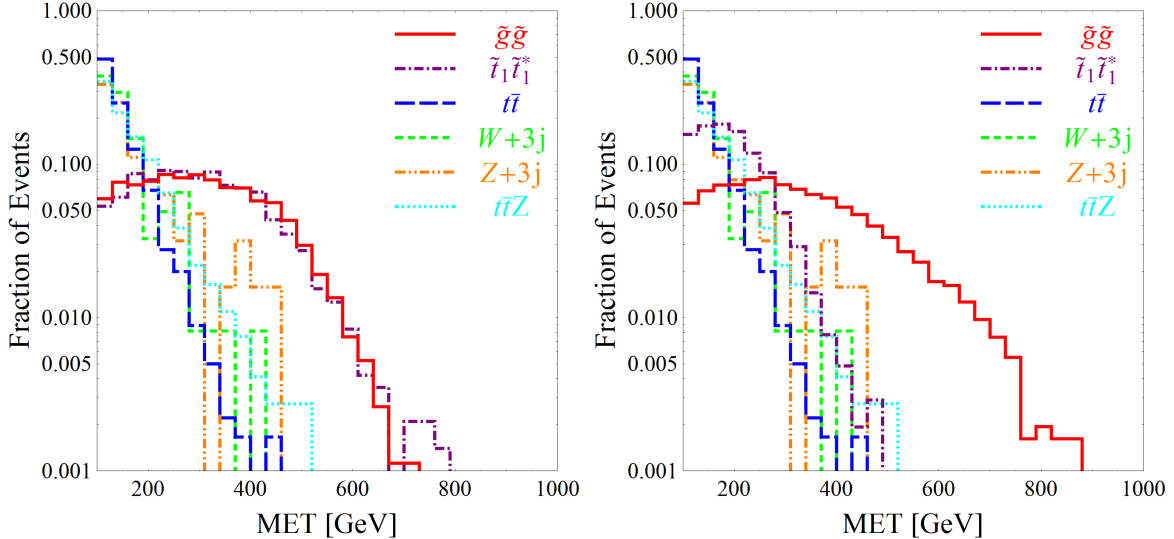


FIG. 5: Event distributions for all relevant signal and background processes as functions of missing transverse energy \cancel{E}_T for two illustrative combinations of the gluino mass $M_{\tilde{g}}$ and stop mass $m_{\tilde{t}_1}$ in our simplified supersymmetric model. The distributions shown in the left panel correspond to the parameter choice $M_{\tilde{g}} = 800$ GeV and $m_{\tilde{t}_1} = 600$ GeV, while those shown in the right panel correspond to $M_{\tilde{g}} = 1200$ GeV and $m_{\tilde{t}_1} = 400$ GeV. As in Fig. 4, each distribution appearing in each panel has been normalized such that the total area under each distribution is unity.

verified from Fig. 2, gluino-pair production provides the dominant signal contribution, and the \cancel{E}_T distributions for both $pp \rightarrow \tilde{g}\tilde{g}$ and $pp \rightarrow \tilde{t}_1\tilde{t}_1^*$ are sufficiently broad compared to those for the SM background processes so as to render an elevated \cancel{E}_T cut an effective discriminant between signal and background. By contrast, the situation displayed in the right panel, which corresponds to the parameter assignments $M_{\tilde{g}} = 1200$ GeV and $m_{\tilde{t}_1} = 400$ GeV, is quite different. Since \tilde{t}_1 is quite light in this case, $pp \rightarrow \tilde{t}_1\tilde{t}_1^*$ provides the dominant signal contribution. However, another consequence of \tilde{t}_1 being so light is that the \tilde{N}_1 produced by stop decay are not particularly energetic. As a result, the \cancel{E}_T distribution for $pp \rightarrow \tilde{t}_1\tilde{t}_1^*$ does not differ as significantly from that of the SM background. We therefore conclude that there is little to be gained by imposing an elevated \cancel{E}_T cut in regions of parameter space in which $m_{\tilde{t}_1}$ is small. On the other hand, an elevated \cancel{E}_T cut does enhance detection prospects for regions of parameter space in which the kinematics of \tilde{t}_1 or \tilde{g} decay is such that substantial kinetic energy is transferred to the \tilde{N}_1 .

In order to provide a more quantitative demonstration of the effects of N_j and \cancel{E}_T cuts on signal and background data, we provide a roster of cross-sections for the various signal and background processes considered in our analysis after the application of different combinations of such cuts in Table II. All cross-sections quoted in this table include the relevant NLO K -factors. In order to demonstrate how the effect of these cuts depends on $M_{\tilde{g}}$ and $m_{\tilde{t}_1}$, we present signal cross-sections for a pair of benchmark scenarios representative of the two principal types of multi-jet phenomenology to which our example model gives rise. For the first of these scenarios, for which $M_{\tilde{g}} = 1000$ GeV and $m_{\tilde{t}_1} = 350$ GeV, the cross-section for the $pp \rightarrow \tilde{t}_1\tilde{t}_1^*$ production process is large enough that this process dominates the event

Cuts	$M_{\tilde{g}} = 1000 \text{ GeV}$ $m_{\tilde{t}_1} = 350 \text{ GeV}$		$M_{\tilde{g}} = 800 \text{ GeV}$ $m_{\tilde{t}_1} = 800 \text{ GeV}$		SM Backgrounds			
	$\tilde{g}\tilde{g}$	$\tilde{t}_1\tilde{t}_1^*$	$\tilde{g}\tilde{g}$	$\tilde{t}_1\tilde{t}_1^*$	$t\bar{t}$ (+jets)	W^\pm (+jets)	Z (+jets)	$t\bar{t}Z$ (+jets)
precuts only	2.04	37.21	15.77	0.16	374.09	66.28	56.86	0.95
$N_j \geq 6$	1.93	23.85	15.09	0.10	194.33	13.04	22.56	0.58
$N_j \geq 7$	1.60	9.47	12.92	0.04	65.54	2.72	6.32	0.24
$N_j \geq 8$	1.11	2.72	8.93	0.01	15.19	0.54	0.90	0.06
$N_j \geq 9$	0.64	0.37	5.01	0	3.75	0	0	0.01
$\cancel{E}_T \geq 200 \text{ GeV}$	1.35	8.06	11.15	0.14	41.47	10.32	15.34	0.23
$N_j \geq 6, \cancel{E}_T \geq 200 \text{ GeV}$	1.28	4.73	10.66	0.08	21.54	1.09	3.61	0.14
$N_j \geq 7, \cancel{E}_T \geq 200 \text{ GeV}$	1.06	1.73	9.07	0.03	7.27	0	0.90	0.06
$N_j \geq 8, \cancel{E}_T \geq 200 \text{ GeV}$	0.73,	0.47	6.20	0.01	1.68	0	0	0.01
$N_j \geq 9, \cancel{E}_T \geq 200 \text{ GeV}$	0.41	0.05	3.38	0	0.42	0	0	0
$\cancel{E}_T \geq 300 \text{ GeV}$	0.71	0.80	5.93	0.11	4.60	1.63	5.42	0.05
$N_j \geq 6, \cancel{E}_T \geq 300 \text{ GeV}$	0.67	0.47	5.65	0.07	2.39	0	0.90	0.03
$N_j \geq 7, \cancel{E}_T \geq 300 \text{ GeV}$	0.55,	0.19	4.79	0.03	0.81	0	0	0.01
$N_j \geq 8, \cancel{E}_T \geq 300 \text{ GeV}$	0.36	0.09	3.26	0.01	0.19	0	0	0
$N_j \geq 9, \cancel{E}_T \geq 300 \text{ GeV}$	0.20	0.05	1.76	0	0.05	0	0	0

TABLE II: Cross-sections (in femtobarns) for the signal processes $pp \rightarrow \tilde{g}\tilde{g}$ and $pp \rightarrow \tilde{t}_1\tilde{t}_1^*$ in a pair of illustrative benchmark scenarios with different values of the model parameters $M_{\tilde{g}}$ and $m_{\tilde{t}_1}$, as well as for the SM backgrounds from $t\bar{t} + \text{jets}$, $W^\pm + \text{jets}$, $Z + \text{jets}$, and $t\bar{t}Z + \text{jets}$ after the application of various cuts. For further details, see text.

rate in the jets + \cancel{E}_T channel. For this scenario, moderate cuts on N_j and \cancel{E}_T similar to those imposed as part of the precuts offer the best prospects for discovery. For the second benchmark scenario, for which $M_{\tilde{g}} = m_{\tilde{t}_1} = 800 \text{ GeV}$, $pp \rightarrow \tilde{g}\tilde{g}$ production dominates, and the best prospects for discovery are obtained by imposing elevated N_j and \cancel{E}_T cuts on the order of $N_j \geq 8$ and $\cancel{E}_T \geq 300 \text{ GeV}$.

VI. PROSPECTS FOR DISCOVERY

The effect of imposing elevated cuts on N_j and \cancel{E}_T on the statistical significance of discovery in different regimes of model-parameter space can be seen in Fig. 6. In this figure, we present a series of contour plots indicating the regions of $(M_{\tilde{g}}, m_{\tilde{t}_1})$ parameter space within which statistically significant evidence of new physics can be obtained at the $\sqrt{s} = 7 \text{ TeV}$ LHC after the application of several different sets of elevated N_j and \cancel{E}_T cuts. All results shown in these panels assume an integrated luminosity $\mathcal{L}_{\text{int}} = 10 \text{ fb}^{-1}$. Since the number of both signal and background events surviving the cuts we impose is often quite small, we calculate the confidence level for all values of $M_{\tilde{g}}$ and $m_{\tilde{t}_1}$ included in our parameter-space survey using Poisson statistics. The significance contours shown in each panel of Fig. 6 are those contours for which the equivalent confidence level for a Gaussian distribution would correspond to a 3σ or 5σ discovery. We also require that the signal is not event-count limited, in the sense that the expected number of signal events at this luminosity which survive all

cuts exceeds five. The gray striped region demarcated by the dashed contour indicates the region of parameter space in which this event-count criterion is not satisfied.

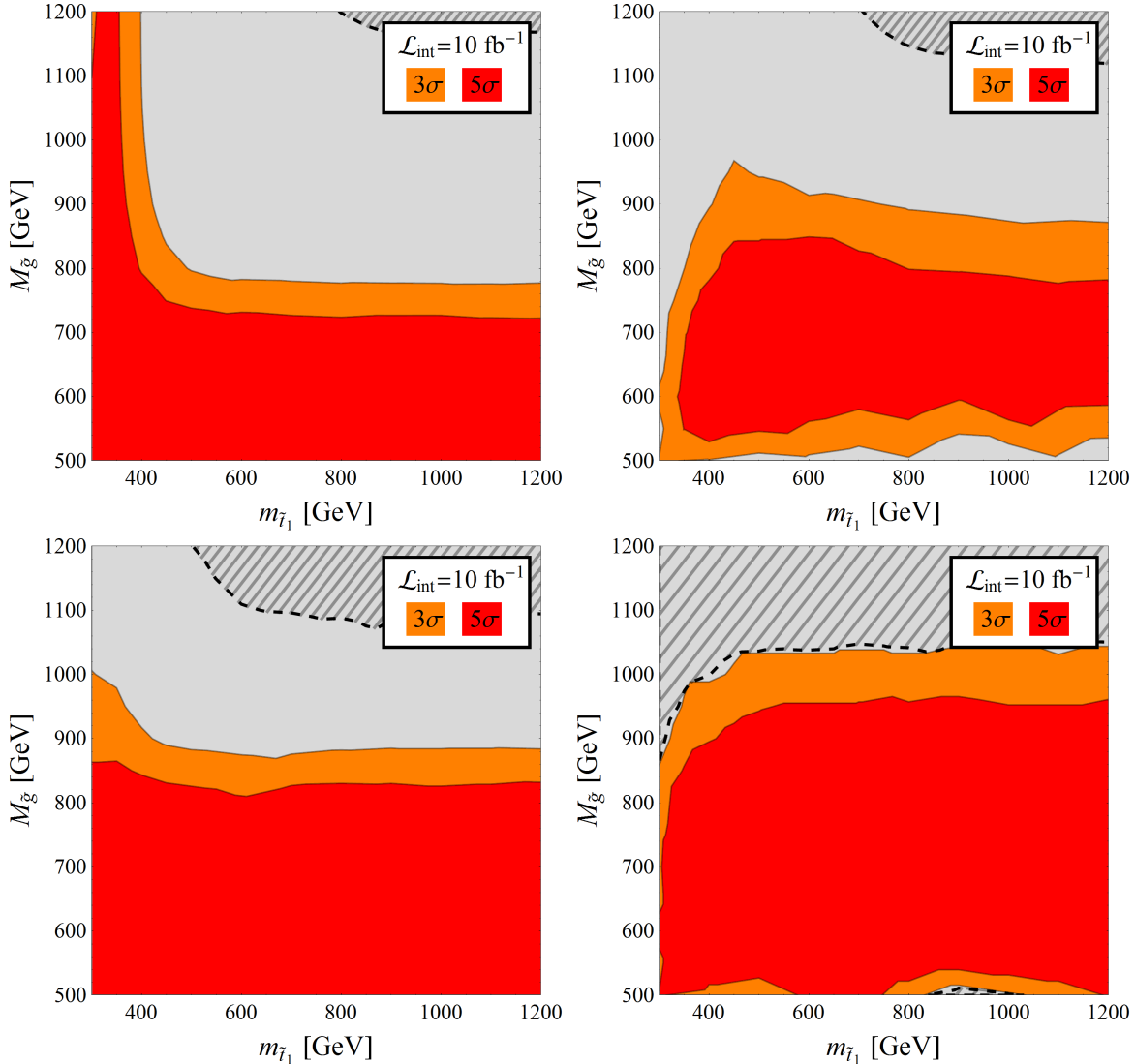


FIG. 6: Contour plots illustrating the regions of $(M_{\tilde{g}}, m_{\tilde{t}_1})$ parameter space within which evidence for new physics can be obtained at the 3σ (orange) or 5σ (red) significance level with $\mathcal{L}_{\text{int}} = 10 \text{ fb}^{-1}$ at the $\sqrt{s} = 7 \text{ TeV}$ LHC after the application of the various sets of cuts discussed in the text. The gray striped region bounded by the dashed contour in each panel demarcates the region within which the expected event count is less than five events at this luminosity. The contours displayed in the upper left panel correspond to the application of the precuts alone. Those in the upper right are obtained by imposing an additional $\cancel{E}_T \geq 300 \text{ GeV}$ cut on top of those precuts, those in the lower left panel are obtained by imposing an additional $N_j \geq 8$ cut on top of the precuts, and those in the lower right panel are obtained by applying these two additional cuts in tandem.

The contours displayed in the upper left panel of Fig. 6 are obtained by imposing the precuts alone. In this case, we see that in the region of parameter space in which $m_{\tilde{t}_1} \lesssim 400 \text{ GeV}$, the signal contribution from $pp \rightarrow \tilde{t}_1 \tilde{t}_1^*$ is substantial, and the $N_j \geq 5$ and p_{T_j} cuts imposed as part of the precuts are sufficient to resolve the signal from this process from the

SM background. Likewise, for $M_{\tilde{g}} \lesssim 725$ GeV, these same cuts alone are also sufficient to resolve the signal from the $pp \rightarrow \tilde{g}\tilde{g}$ process.

The situation changes, however, when the minimum \cancel{E}_T threshold is elevated, as is evident from the upper right panel of Fig. 6. This panel displays the results obtained by imposing an additional $\cancel{E}_T \geq 300$ GeV cut on top of the $\cancel{E}_T \geq 100$ GeV requirement included as part of the precuts. These results indicate that in regions of parameter space in which $M_{\tilde{g}} \gg 2m_t + M_{\tilde{N}_1}$, for which neutralinos produced via the $pp \rightarrow \tilde{g}\tilde{g}$ process tend to be quite energetic, \cancel{E}_T serves as an extremely effective criterion for distinguishing signal from background, as we also saw in Fig. 5. (An exception occurs in cases in which $M_{\tilde{g}} \gg m_{\tilde{t}_1}$ and the top quarks receive a greater proportion of the mass energy of the decaying gluino.) The same is true of neutralinos produced via the $pp \rightarrow \tilde{t}_1\tilde{t}_1^*$ process in regions of parameter space in which $m_{\tilde{t}_1} \gg m_t + M_{\tilde{N}_1}$. Conversely, when these conditions on $M_{\tilde{g}}$ and $m_{\tilde{t}_1}$ are not satisfied, \cancel{E}_T serves as a poor discriminant between the respective $pp \rightarrow \tilde{g}\tilde{g}$ and $pp \rightarrow \tilde{t}_1\tilde{t}_1^*$ signal contributions and the SM background, and the significance of discovery afforded by the corresponding signal process decreases.

The lower left panel of Fig. 6 displays the results obtained by imposing an additional $N_j \geq 8$ cut in addition to the precuts. Events produced by $pp \rightarrow \tilde{g}\tilde{g}$, for which the characteristic jet multiplicity is quite high, tend to survive such a cut, which is quite efficient in eliminating events from the SM backgrounds. For this reason, the discovery potential afforded by this signal process is improved with each incremental increase in the N_j requirement up to a reasonably high threshold — unless other considerations, such as the total expected number of signal events, become an issue. In accord with the results displayed in Fig. 4, we find that this threshold occurs for a cut in the $N_j \gtrsim 8 - 10$ range. By contrast, events produced by $pp \rightarrow \tilde{t}_1\tilde{t}_1^*$ tend to involve far lower jet multiplicities; hence substantially elevating the N_j cut results in a loss of significance in those regions of parameter space within which this process is responsible for the dominant signal contribution.

The lower right panel of Fig. 6 displays the results obtained by imposing both an $N_j \geq 8$ cut and a $\cancel{E}_T \geq 300$ GeV cut in addition to the precuts. This set of cuts yields a 5σ significance throughout a broad region of parameter space within which 550 GeV $\lesssim M_{\tilde{g}} \lesssim 950$ GeV. This clearly constitutes a far greater reach than that obtained by imposing either an elevated N_j cut or an elevated \cancel{E}_T cut alone. As before, the elevated N_j cut results in the signal rate being dominated by gluino-pair production, as expected. It is also evident from the results displayed in this panel that at $\mathcal{L}_{\text{int}} = 10 \text{ fb}^{-1}$, the effect of the combined \cancel{E}_T and N_j cuts imposed here on the signal-event rate is quite severe. Indeed, we find that further increasing the jet-multiplicity threshold beyond $N_j \geq 8$ or substantially elevating the \cancel{E}_T cut above $\cancel{E}_T \geq 300$ GeV does not result in a significant improvement in the reach, essentially because the signal becomes event-count limited.

In addition to the statistical significance of discovery itself, the signal-to-background ratio S/B is also of interest, since estimates of that significance can be unreliable for large S/B due to systematic uncertainties in the expected backgrounds. For each combination of elevated N_j and \cancel{E}_T cuts considered in Fig. 6, we have verified that for $S/B \geq 0.1$ throughout all regions of parameter space shown in that figure within which a significance of 3σ or above is obtained. This suggests that our results are indeed robust against systematic uncertainties affecting the background. Indeed, only for the precuts alone do we find that this criterion on S/B is not satisfied, and only within certain regions of parameter space within which $m_{\tilde{t}_1} \ll M_{\tilde{g}}$.

One can compare these results to those afforded by other, complementary strategies [23,

25] for observing a signal of new physics from a pair of gluinos decaying into $t\bar{t}\bar{t}\bar{t} + \cancel{E}_T$. From among those strategies, the best reach is obtained by demanding one lepton and four b -tagged jets in the final state [25], which permits a 5σ discovery for $M_{\tilde{g}}$ as high as 650 GeV at an integrated luminosity of 1 fb^{-1} . By contrast, with the search strategy we adopt here — and specifically by requiring that $N_j \geq 8$ and $\cancel{E}_T \geq 200 \text{ GeV}$ — we find that the LHC reach (at the same significance level and with the same luminosity) can be increased to roughly 730 GeV. This serves as just one example of how a search strategy focused on fully hadronic events with large jet multiplicities and substantial \cancel{E}_T can be useful in identifying signals of new physics in top-rich scenarios at the LHC.

To summarize the qualitative results of this section, we find that in situations in which $pp \rightarrow \tilde{g}\tilde{g}$ production dominates, focusing on high-jet-multiplicity events in the fully hadronic channel is an effective strategy for uncovering new physics at the LHC. By contrast, we find that in situations in which $pp \rightarrow \tilde{t}_1\tilde{t}_1^*$ production (a process for which the characteristic jet multiplicities are far lower) dominates, this strategy is far less effective. These results therefore provide insight into what sorts of scenarios are likely to benefit from such a search strategy, and what sorts of models may be less amenable to such techniques.

VII. CONCLUSIONS

In this paper, we have investigated the potential for identifying signals of new physics at the LHC using a search strategy which focuses on the jets + \cancel{E}_T channel and uses N_j and \cancel{E}_T as the principal criteria for resolving such signals from the SM background. This approach is particularly suitable in top-rich scenarios, which generically give rise to events with large jet multiplicities. To demonstrate the effectiveness of this search strategy in such scenarios, we have examined the detection prospects it affords in an example model whose field content comprises a gluino \tilde{g} , a light, right-handed stop \tilde{t}_1 , and a bino-like neutralino \tilde{N}_1 . We have shown that for this model, the discovery reach provided by this search strategy is comparable to — and potentially greater than — that afforded by other strategies for identifying top-rich new physics at the LHC. These preliminary results provide compelling motivation for a more detailed analysis of this discovery reach — an analysis which takes into account more fully the various experimental subtleties (detector effects, calibration issues, *etc.*) involved.

While we have focused on this specific model in order to demonstrate the effectiveness of a search strategy focused on N_j and \cancel{E}_T , we note that similar results can be expected for a broad class of top-rich scenarios. These include models with additional fermion generations, SUSY scenarios featuring light stops and heavy first- and second-generation squarks (including certain string-theory-inspired scenarios [30, 31]), Little Higgs models with T-parity, UED models, and a variety of other new-physics scenarios. Our results serve as motivation for more detailed studies of the discovery potential for new physics using such a search strategy in such contexts — especially those in which decay topologies for the heavy fields involve top quarks and invisible particles almost exclusively. Indeed, in the time since this paper initially appeared, some studies of this sort [59] have been undertaken by the ATLAS collaboration.

The optimal program of event-selection criteria for any given scenario (and the detection prospects it affords) of course depends on the production rates for any new strongly-interacting fields involved, and hence on the masses, spins, and $SU(3)_c$ representations of those fields. They also depend quite sensitively on the structure of the decay chains initi-

ated by those new strongly-interacting fields and on the kinematics of the final-state particles which result from each decay. For example, the effectiveness of \cancel{E}_T as an event-selection criterion in any particular scenario depends on how much of the energy released by particle decays emerges in the form of jets and how much emerges in the form of invisible particles. This balance depends sensitively on the structures and kinematics of the decay chains involved, and the more this balance is tilted toward invisible particles, the more effective a discriminant a \cancel{E}_T cut will generally become. The optimal event-selection criteria depend on other factors as well. For example, at $\mathcal{L}_{\text{int}} = 10 \text{ fb}^{-1}$ and $\sqrt{s} = 7 \text{ TeV}$, we find that there is no advantage to requiring more than eight energetic jets or \cancel{E}_T significantly in excess of 300 GeV, since further elevating the cuts on these variables tends to reduce the expected number of signal events to a negligible level. However, for higher \mathcal{L}_{int} or a larger \sqrt{s} (as is expected in the coming LHC run), further increasing the N_j and \cancel{E}_T thresholds cuts beyond those levels may indeed prove fruitful.

On a final note, we mention another potentially interesting strategy which could be useful in identifying signals of new physics in certain top-rich scenarios, and which can be viewed as complementary to the strategy outlined here. This is to focus on final states involving bottom quarks plus \cancel{E}_T alone. The utility of this approach was investigated in Ref. [60] in the context of a model with an additional pair of color-triplet fermions T' and B' , which decay almost exclusively via the channels $T' \rightarrow tX$ and $B' \rightarrow bX$, where X is a stable dark-matter particle. It was found that for $m_X \sim 1 \text{ GeV}$, the $pp \rightarrow B'\bar{B}' \rightarrow b\bar{b} + \cancel{E}_T$ and $pp \rightarrow T'\bar{T}' \rightarrow t\bar{t} + \cancel{E}_T$ channels offered a comparable reach. Furthermore, it was argued that improved sensitivity in the $b\bar{b} + \cancel{E}_T$ channel can be expected as m_X increases, provided that the T' is reasonably light, since when this is the case, the jets produced from top decay tend to be reasonably soft. This scenario was analyzed in a recent study by the ATLAS collaboration at an integrated luminosity of 0.83 fb^{-1} [61]. In this study, the collaboration searched for evidence of gluino-pair production followed by the decay $\tilde{g} \rightarrow b\bar{b}\tilde{N}_1$, assuming a branching fraction for this process of effectively unity. For $m_{\tilde{g}} < 600 \text{ GeV}$ and a neutralino mass set to $M_{\tilde{N}_1} = 60 \text{ GeV}$, the results of this study place a bound $M_{\tilde{g}} \gtrsim 725 \text{ GeV}$ on the gluino mass, which is roughly comparable to the expected 5σ sensitivity the search strategy we have outlined in this paper for models in which the primary decay channel for the gluino is $\tilde{g} \rightarrow t\bar{t}\tilde{N}_1$. It would be interesting to consider how the discovery prospects afforded by these two approaches compare in models in which *both* $\tilde{g} \rightarrow b\bar{b}\tilde{N}_1$ and $\tilde{g} \rightarrow t\bar{t}\tilde{N}_1$ channels have sufficient branching fraction — to wit, models which involve not only top-rich, but also bottom-rich event topologies.

VIII. ACKNOWLEDGMENTS

We gratefully acknowledge J. Alwall, A. Rajaraman, J. Rutherford, S. Su, X. Tata, and D. Yaylali for useful discussions. This work is supported in part by the Department of Energy under Grant No. DE-FG02-04ER41291 and by the National Science Foundation under Grant No. 1066293. J. K. would also like to thank the Aspen Center for Physics for

its hospitality during the period in which this work was being completed.

-
- [1] R. S. Chivukula, M. Golden, and E. H. Simmons, Nucl. Phys. **B363**, 83-96 (1991); Phys. Lett. **B257**, 403 (1991).
 - [2] R. Essig, Ph.D. thesis, AAT-3349692, PROQUEST-1692394711. Oct 2008.
 - [3] J. Kumar, A. Rajaraman and B. Thomas, Phys. Rev. D **84**, 115005 (2011) [arXiv:1108.3333 [hep-ph]].
 - [4] T. Aaltonen *et al.* [CDF Collaboration], Phys. Rev. Lett. **107**, 042001 (2011) [arXiv:1105.2815 [hep-ex]].
 - [5] S. Chatrchyan *et al.* [CMS Collaboration], Phys. Rev. Lett. **107**, 101801 (2011) [arXiv:1107.3084 [hep-ex]].
 - [6] G. Servant and T. M. P. Tait, Nucl. Phys. B **650**, 391 (2003) [arXiv:hep-ph/0206071]; H. C. Cheng, J. L. Feng, and K. T. Matchev, Phys. Rev. Lett. **89**, 211301 (2002) [arXiv:hep-ph/0207125].
 - [7] I. Antoniadis, Phys. Lett. B **246**, 377 (1990);
I. Antoniadis, K. Benakli, and M. Quiros, Phys. Lett. B **331**, 313 (1994) [arXiv:hep-ph/9403290].
 - [8] K. R. Dienes, E. Dudas, and T. Gherghetta, Phys. Lett. B **436**, 55 (1998) [arXiv:hep-ph/9803466]; Nucl. Phys. B **537**, 47 (1999) [arXiv:hep-ph/9806292]; arXiv:hep-ph/9807522.
 - [9] T. Appelquist, H. C. Cheng, and B. A. Dobrescu, Phys. Rev. D **64**, 035002 (2001) [arXiv:hep-ph/0012100].
 - [10] H. C. Cheng and I. Low, JHEP **0309**, 051 (2003) [arXiv:hep-ph/0308199]; JHEP **0408**, 061 (2004) [arXiv:hep-ph/0405243].
 - [11] N. Arkani-Hamed, A. G. Cohen, and H. Georgi, Phys. Lett. B **513**, 232 (2001) [arXiv:hep-ph/0105239].
 - [12] J. L. Feng and J. Kumar, Phys. Rev. Lett. **101**, 231301 (2008) [arXiv:0803.4196 [hep-ph]];
J. L. Feng, J. Kumar, and L. E. Strigari, Phys. Lett. B **670**, 37 (2008) [arXiv:0806.3746 [hep-ph]];
B. Dutta and J. Kumar, Phys. Lett. B **699**, 364 (2011) [arXiv:1012.1341 [hep-ph]];
P. Fileviez Perez and M. B. Wise, Phys. Rev. D **82**, 011901 (2010) [Erratum-ibid. D **82**, 079901 (2010)] [arXiv:1002.1754 [hep-ph]];
T. R. Dulaney, P. Fileviez Perez, and M. B. Wise, Phys. Rev. D **83**, 023520 (2011) [arXiv:1005.0617 [hep-ph]].
 - [13] V. M. Abazov *et al.* [D0 Collaboration], Phys. Lett. B **660**, 449 (2008) [arXiv:0712.3805 [hep-ex]].
 - [14] T. Aaltonen *et al.* [CDF Collaboration], Phys. Rev. Lett. **102**, 121801 (2009) [arXiv:0811.2512 [hep-ex]].
 - [15] T. Aaltonen *et al.* [CDF Collaboration], Phys. Rev. Lett. **105**, 131801 (2010) [arXiv:0912.4691 [hep-ex]].
 - [16] V. Khachatryan *et al.* [CMS Collaboration], Phys. Lett. B **698**, 196 (2011) [arXiv:1101.1628 [hep-ex]].
 - [17] J. B. G. da Costa *et al.* [Atlas Collaboration], Phys. Lett. B **701**, 186 (2011) [arXiv:1102.5290 [hep-ex]]; ATLAS-CONF-2011-086.

- [18] ATLAS Collaboration, ATLAS-CONF-2011-086.
- [19] S. Chatrchyan *et al.* [CMS Collaboration], Phys. Rev. Lett. **107**, 221804 (2011) [arXiv:1109.2352 [hep-ex]].
- [20] K. R. Dienes and B. Thomas, Phys. Rev. D **85**, 083523 (2012) [arXiv:1106.4546 [hep-ph]]; Phys. Rev. D **85**, 083524 (2012) [arXiv:1107.0721 [hep-ph]].
- [21] P. Meade and M. Reece, Phys. Rev. D **74**, 015010 (2006) [arXiv:hep-ph/0601124]; T. Han, R. Mahbubani, D. G. E. Walker, and L. T. E. Wang, JHEP **0905**, 117 (2009) [arXiv:0803.3820 [hep-ph]].
- [22] J. Alwall, J. L. Feng, J. Kumar, and S. Su, Phys. Rev. D **81**, 114027 (2010) [arXiv:1002.3366 [hep-ph]].
- [23] M. Toharia, J. D. Wells, JHEP **0602**, 015 (2006). [hep-ph/0503175].
- [24] B. S. Acharya, P. Grajek, G. L. Kane, E. Kuflik, K. Suruliz, and L. T. Wang, arXiv:0901.3367 [hep-ph].
- [25] G. L. Kane, E. Kuflik, R. Lu and L. -T. Wang, Phys. Rev. D **84**, 095004 (2011) [arXiv:1101.1963 [hep-ph]].
- [26] K. M. Cheung, arXiv:hep-ph/9507411; M. Spira and J. D. Wells, Nucl. Phys. B **523**, 3 (1998) [arXiv:hep-ph/9711410]; A. Djouadi, G. Moreau, and R. K. Singh, Nucl. Phys. B **797**, 1 (2008) [arXiv:0706.4191 [hep-ph]]; M. Guchait, F. Mahmoudi, and K. Sridhar, Phys. Lett. B **666**, 347 (2008) [arXiv:0710.2234 [hep-ph]]; B. Lillie, J. Shu, and T. M. P. Tait, JHEP **0804**, 087 (2008) [arXiv:0712.3057 [hep-ph]]; A. Pomarol and J. Serra, Phys. Rev. D **78**, 074026 (2008) [arXiv:0806.3247 [hep-ph]]; M. Battaglia and G. Servant, arXiv:1005.4632 [hep-ex]; S. Jung and J. D. Wells, JHEP **1011**, 001 (2010) [arXiv:1008.0870 [hep-ph]].
- [27] C. Englert, T. Plehn, P. Schichtel and S. Schumann, Phys. Rev. D **83**, 095009 (2011) [arXiv:1102.4615 [hep-ph]].
- [28] A. Hook, E. Izaguirre, M. Lisanti and J. G. Wacker, Phys. Rev. D **85**, 055029 (2012) [arXiv:1202.0558 [hep-ph]].
- [29] T. Aaltonen *et al.* [CDF Collaboration], Phys. Rev. Lett. **107**, 191803 (2011) [arXiv:1107.3574 [hep-ex]].
- [30] T. Li, J. A. Maxin, D. V. Nanopoulos and J. W. Walker, Phys. Rev. D **84**, 076003 (2011) [arXiv:1103.4160 [hep-ph]].
- [31] T. Li, J. A. Maxin, D. V. Nanopoulos and J. W. Walker, arXiv:1108.5169 [hep-ph].
- [32] D. Alves *et al.*, arXiv:1105.2838 [hep-ph].
- [33] S. Dawson, E. Eichten, and C. Quigg, Phys. Rev. D **31**, 1581 (1985).
- [34] A. Kulesza and L. Motyka, Phys. Rev. D **80**, 095004 (2009) [arXiv:0905.4749 [hep-ph]].
- [35] J. Pumplin, D. R. Stump, J. Huston, H. L. Lai, P. M. Nadolsky, and W. K. Tung, JHEP **0207**, 012 (2002) [arXiv:hep-ph/0201195].
- [36] W. Beenakker, R. Hopker, M. Spira, and P. M. Zerwas, Nucl. Phys. B **492**, 51 (1997) [arXiv:hep-ph/9610490]; W. Beenakker, M. Kramer, T. Plehn, M. Spira, and P. M. Zerwas, Nucl. Phys. B **515**, 3 (1998) [arXiv:hep-ph/9710451].
- [37] W. Beenakker, S. Brensing, M. Kramer, A. Kulesza, E. Laenen, and I. Niessen, JHEP **0912**, 041 (2009) [arXiv:0909.4418 [hep-ph]]; W. Beenakker, S. Brensing, M. Kramer, A. Kulesza, E. Laenen, L. Motyka, and I. Niessen,

- Int. J. Mod. Phys. A **26**, 2637 (2011) [arXiv:1105.1110 [hep-ph]].
- [38] T. Plehn, D. Rainwater, and P. Z. Skands, Phys. Lett. B **645**, 217 (2007) [arXiv:hep-ph/0510144].
- [39] G. Aad *et al.* [Atlas Collaboration], Phys. Rev. Lett. **106**, 131802 (2011) [arXiv:1102.2357 [hep-ex]].
- [40] G. Aad *et al.* [ATLAS Collaboration], Phys. Lett. B **701**, 398 (2011) [arXiv:1103.4344 [hep-ex]].
- [41] T. Aaltonen *et al.* [CDF Collaboration], Phys. Rev. Lett. **106**, 191801 (2011) [arXiv:1103.2482 [hep-ex]].
- [42] ATLAS Collaboration, ATLAS-CONF-2011-036.
- [43] G. Aad *et al.* [ATLAS Collaboration], Phys. Rev. Lett. **108**, 041805 (2012) [arXiv:1109.4725 [hep-ex]].
- [44] T. Aaltonen *et al.* [CDF Collaboration], Phys. Rev. **D82**, 092001 (2010). [arXiv:1009.0266 [hep-ex]].
- [45] V. M. Abazov *et al.* [D0 Collaboration], Phys. Lett. **B675**, 289-296 (2009). [arXiv:0811.0459 [hep-ex]].
- [46] A. G. Ivanov [CDF Collaboration], arXiv:0811.0788 [hep-ex].
- [47] A. Djouadi, J. L. Kneur, and G. Moultaka, Comput. Phys. Commun. **176**, 426 (2007) [arXiv:hep-ph/0211331].
- [48] J. Alwall *et al.*, JHEP **0709**, 028 (2007) [arXiv:0706.2334 [hep-ph]].
- [49] T. Sjostrand, S. Mrenna, and P. Skands, JHEP **0605**, 026 (2006) [arXiv:hep-ph/0603175].
- [50] “PGS – Pretty Good Simulator”,
<http://www.physics.ucdavis.edu/~conway/research/software/pgs/pgs4-general.html>
- [51] V. M. Abazov *et al.* [D0 Collaboration], Phys. Lett. B **638**, 119 (2006) [arXiv:hep-ex/0604029].
- [52] ATLAS Collaboration, ATL-PHYS-PUB-2009-084.
- [53] C. F. Berger *et al.*, Nucl. Phys. Proc. Suppl. **205-206**, 92 (2010) [arXiv:1005.3728 [hep-ph]].
- [54] C. F. Berger *et al.*, Phys. Rev. D **80**, 074036 (2009) [arXiv:0907.1984 [hep-ph]].
- [55] J. M. Campbell, J. W. Huston, and W. J. Stirling, Rept. Prog. Phys. **70**, 89 (2007) [arXiv:hep-ph/0611148].
- [56] Z. Bern *et al.* [NLO Multileg Working Group], arXiv:0803.0494 [hep-ph].
- [57] A. Lazopoulos, T. McElmurry, K. Melnikov, and F. Petriello, Phys. Lett. B **666**, 62 (2008) [arXiv:0804.2220 [hep-ph]].
- [58] CMS Collaboration, CMS-PAS-SUS-11-003.
- [59] G. Aad *et al.* [Atlas Collaboration], JHEP **1111**, 099 (2011) [arXiv:1110.2299 [hep-ex]].
- [60] J. Alwall, J. L. Feng, J. Kumar and S. Su, Phys. Rev. D **84**, 074010 (2011) [arXiv:1107.2919 [hep-ph]].
- [61] B. Butler for the ATLAS Collaboration, arXiv:1109.4707 [hep-ex].